*–Demonstration–*

# Real-Time Sliding Mode Observer Scheme for Shear Force Estimation in a Transverse Dynamic Force Microscope

Thang Nguyen[1], Said G Khan[2], Toshiaka Hatano[2], Kaiqiang Zhang[2], Christopher Edwards[1], Guido Herrmann[2], Robert Harniman[3], Stuart C. Burgess[2], Massimo Antognozzi[3] and Mervyn Miles[3]

## ABSTRACT

This paper describes a sliding mode observer scheme for estimation of the shear force affecting the cantilever in a *Transverse Dynamic Force Microscope* (TDFM). The vertically oriented cantilever is oscillated in proximity to the specimen under investigation. The amplitude of oscillation of the cantilever tip is affected by these shear forces. They are created by the ordered-water layer above the specimen. The oscillation amplitude is therefore a measure of distance between the tip and the surface of the specimen. Consequently, the estimation of the shear forces provides useful information about the specimen characteristics. For estimating the shear forces, an approximate finite dimensional model of the cantilever is created using the method of lines. This model is subsequently reduced for its model order. An unknown input sliding mode observer has been used to reconstruct the unknown shear forces using only tip position measurements and the cantilever excitation. This paper describes the development of the sliding mode scheme and presents experimental results from the TDFM set up at the Centre for Nanoscience and Quantum Information (NSQI) at Bristol University.

***Key Words:*** Transverse Dynamic Force Microscope, Nano Systems

## I. INTRODUCTION

The Atomic Force Microscope (AFM) is an important instrument for investigating specimens at nano-scale. These devices can provide high resolution images in ambient, aqueous and vacuum environments, and consequently are invaluable for studying biological specimens under physiological conditions. In traditional contact AFM with a horizontal cantilever arrangement, the (force) interaction between the cantilever tip and the specimen is inferred by the induced bending of the cantilever. The bending of the cantilever, when obtained at different positions as part of a raster scan of the sample surface, creates a high resolution topographical image.

Significant advances have been made in terms of achieving higher temporal resolution through improved electronics in conjunction with sophisticated control approaches [1, 23, 29, 30], stable fast-scan sample stages [38], and by miniaturising cantilevers [25]. In particular, the miniaturisation of cantilevers increases their resonance frequency, and thus increases the bandwidth of the detection system [21].

Most AFMs are set up in such a way that the cantilever is oscillated in the horizontal plane, and they operate in a tapping mode [27, 35] or contact mode [29, 38]. In contrast, the *Transverse Dynamic Force Microscope* (TDFM) at Bristol addresses the issue of non-contact imaging. The setup at Bristol employs

Manuscript received July 8, 2015.

[1] College of Engineering, Mathematics and Physical Sciences, University of Exeter, Exeter UK EX4 4QF, UK; Corresponding Author at Exeter: C.Edwards@exeter.ac.uk; [2] Department of Mechanical Engineering, University of Bristol, University Walk, Bristol, BS8 1TR, UK; Corresponding Author at Bristol: G.Herrmann@bris.ac.uk; [3] Centre for Nanoscience and Quantum Information, University of Bristol, Tyndall Avenue, Bristol, BS8 1FD, UK;

This research is supported under the EPSRC grants EP/I034882/1 & EP/I034831/1

a vertically oriented cantilever (VOC) with a length of 28 $\mu$m and a first modal frequency of 353 kHz. The surface is identified by observing changes in the cantilever resonant dynamics. The vertical orientation of the cantilever prevents the 'snap-to-contact' effect experienced by conventional AFM cantilevers when the gradient of the surface attractive force becomes larger than the spring constant of the cantilever [7]. This results in the possibility of operating the TDFM in a non-contact fashion allowing delicate biological specimens to be tested in situ.

It can be seen from the arguments above, the cantilever probe in the TDFM (or indeed in AFMs in general) is a vital component of the device. The (dynamic) changes in the cantilever during its interaction with the specimen indirectly captures a wealth of information related to the mechanical characteristics of the specimen. Hence, understanding the dynamic behaviour of the cantilever in real-time and identifying key model parameters is very beneficial. Unsurprisingly, the problem of estimating the cantilever parameters has been investigated by many researchers. Besancon *et al.* [6] considered an observer-based approach to estimate unknown forces affecting the dynamics of a cantilever in *Electric Force Microscopy* devices. De *et al.* [10] proposed a real-time scheme to determine the probe loss areas in atomic force microscopy using imaging systems based on tapping modes. Later, Xu *et al.* [43] studied a two degree of freedom mathematical model of a tapping mode AFM when the cantilever is immersed in liquid, from which the tip-sample interaction forces are estimated. For horizontally oriented cantilevers, the team of Jalili, has developed a series of interesting results for estimation and control in simulated AFM problems using a lumped parameter model [19, 20] and also a distributed model [16]. In these results, the output signal derivative is needed. Jalili and co-workers also tested an experimental controller for a relatively large cantilever with resonance frequencies below 3 kHz using a distributed cantilever model [17]. Also practical studies for the identification of a distributed model have been carried out in [18] for a cantilever with resonance frequencies below 55 kHz.

In contrast to much of the AFM research literature described above (which uses horizontally oriented cantilevers), in this paper, the problem of estimating the tip-sample interaction forces is associated with a regime in which the cantilever probe is vertically orientated. The practical problem addressed in this paper is very challenging, because the techniques need to work for cantilevers with resonance frequencies well above 300 KHz. Thus, the complexity of the techniques which can be applied practically is very constrained.

In this paper, a robust process is suggested which allows the estimation of the shear force arising from the interaction of the cantilever-tip and the sample. The top of the vertical cantilever is excited to detect the dynamics resulting from the shear force at the tip. Thus, the excitation signal and the shear force are not physically collocated. This requires the development of a mathematical model of the cantilever to understand the dynamic interaction of the excitation and the shear force through the cantilever. A robust process is suggested which allows the application of a sliding mode observer, based on a low order linear model, avoiding the requirement of any extra measurements such as the cantilever tip velocity. It is well established that sliding mode observers are a possible robust solution to this problem in comparison to many other options [8, 9, 12, 24, 28, 32, 42]. Sliding mode observers exhibit a high degree of accuracy when estimating state variables in the presence of unknown inputs [14, 22, 39]. For this reason, there is increasing use of these ideas in the area of fault detection and isolation. In particular, sliding mode observers can be used to simultaneously estimate within finite time both internal states and unknown inputs [15] without needing to impose restrictions on the unknown signal (see for example [8]). This is helpful since the unknown shear force is created by the nonlinear, partially discontinuous, characteristics of the thin ordered layer of water molecules above the specimen. In this paper, an observer will be designed based on the method originally proposed in [14], where the so-called equivalent output injection signal is exploited to accurately reconstruct the unknown tip-sample shear force.

Thus, in the paper a mathematical model of the TDFM cantilever will be introduced in which the dynamics take the form of a 4th order partial differential equation (PDE). The method of lines is then employed to extract a system of ordinary differential equations (ODEs), representing a high order linear time invariant system relating the tip position to the shear forces and the external excitation. Model order reduction is then employed to obtain a simple lower order model. A sliding mode observer based on the reduced order model is then used to reconstruct the unknown tip-sample interaction force.

There are two main contributions in terms of research in this paper. Firstly, it proposes a practical process to design and synthesize an estimation scheme using sliding mode techniques. For this purpose,

an ODE model is derived from the spatio-temporal PDE description of the dynamics of the vertically oriented cantilever, and then a sliding mode observer is suggested and designed to estimate the tip-sample interaction force. Secondly, the process is practically demonstrated, which is novel in terms of this realm of application.

The paper is organised as follows. Section II discusses the problem formulation and introduces the mathematical model of the dynamics of the TDFM cantilever probe in the form of a PDE. In Section III, the method of lines and model order reduction are employed to obtain a finite dimensional model. A sliding mode observer for the reduced order model is then described in Section IV. Experimental results are demonstrated in Section V and conclusions are drawn in Section VI.

## II. The Transverse Dynamic Force Microscope - Problem formulation

Bristol's TDFM consists of two main (mechanical) parts: the head and the adjustable platform which carries the specimen. A sub-micron specimen is mounted on a transparent substrate, typically a glass coverslip of thickness less than $130\ \mu m$. The substrate is then attached to two X-Y translation stages: the first X-Y translation stage (Physik Instrumente P-734) has a central aperture and a scan range of $100\ \mu m$; and the second high speed X-Y stage, on top of the P-734, increases the overall bandwidth. The sample is then translated to create the surface image following a typical raster scan pattern.

The head carries the vertically oriented cantilever which is actuated in the z-direction by two piezo-actuators. These provide fine and coarse resolution respectively (see the simplified representation of the TDFM in Figure 1). The cantilever is sinusoidally oscillated in the vertical direction by a third piezo actuator at a frequency close to its fundamental flexural mode, and typically with an amplitude of less than 2 nm. As the tip is lowered towards the surface, a shear force interaction produces a reduction in the oscillation amplitude, measured on the photo-detector. A schematic of the TDFM setup is shown in Figure 1. In this setup, laser light is emitted from a source (A) and is focussed through the objective lens (B). This has the effect of illuminating the bio-specimen from below and produces an exponentially decaying evanescent field above the specimen, which is used to measure the vibration amplitude [26]. When the cantilever probe tip enters the evanescent field above the specimen, the tip of the cantilever illuminates and light is scattered, also reaching the optical lens (B). A complex optical mechanism (SEW) [3] extracts from the scattered light the vibration amplitude.

The TDFM exploits the shear force interaction that happens in the thin ordered water layer close to the specimen (usually a biomolecule) surface (Figure 2). The hydrodynamic properties of this thin layer of water (usually only a few nano metres thick) significantly influences the amplitude of the cantilever tip. This water layer is usually also present in specimens, which are not immersed in a fluid, e.g. non-biological specimens. As experiments are usually conducted at normal ambient room conditions (in terms of temperature, pressure and humidity), a thin ordered water layer always exists due to humidity. As the cantilever interacts with the water layer, the closer the cantilever tip is to the specimen, the greater the shear force exerted by the ordered water layer. This decreases the amplitude of oscillation of the cantilever tip. Thus, the vibration amplitude and the shear force are an excellent measure of specimen-cantilever distance.

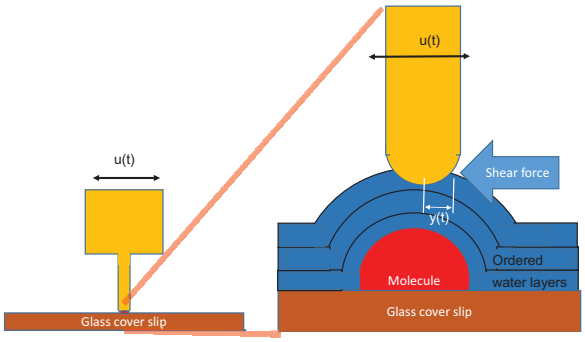


Fig. 2. The TDFM-cantilever in bulkwater & cantilever tip in interaction with the ordered layers.

The next Section develops a partial differential equation (PDE) model of the cantilever which is the starting point for the development of the observer based scheme.

### 2.1. Spatio-temporal cantilever model

To model the cantilever shear force interaction [2, 4], the spatio-temporal dynamics can be presented in the form

$$\frac{\partial^4 EI(Y+\alpha\dot{Y})}{\partial\zeta^4} + \rho A_s \ddot{Y} + \gamma w \dot{Y} = 0 \qquad (1)$$

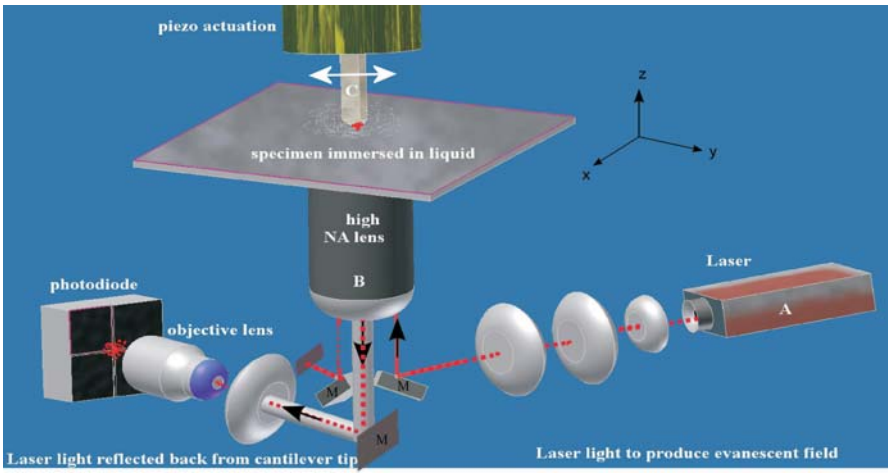


Fig. 1. Simplified schematic of the TDFM together with SEW system (adopted from [26]).

with boundary conditions

$$Y(\zeta = 0) = u(t) = d_0 \sin(\omega t), \quad (2)$$

$$\frac{\partial Y}{\partial \zeta}(\zeta = 0) = 0, \quad (3)$$

$$\frac{\partial^2 Y}{\partial \zeta^2}(\zeta = L) = 0, \quad (4)$$

$$EI\frac{\partial^3 Y}{\partial \zeta^3}(\zeta = L) = -f(t), \quad (5)$$

where $E$ is Young's modulus, $\alpha$ is the internal damping constant of the cantilever, $I$ is the secondary moment of area, $A_s$ is the cross-sectional area, $\rho$ is the density of the probe, $L$ is the length of the cantilever, $w$ is the width of the cantilever, $\zeta$ denotes position along the probe axis, $Y$ is the transversal displacement at any point along the probe during vibration. The scalar $\gamma$ is the damping coefficient of the surrounding fluid, in which the cantilever might be fully immersed. This is the case for inspection of biological samples (for example), while for 'dry' samples $\gamma = 0$. In (1), $\dot{Y}$ and $\ddot{Y}$ are the first and second derivatives of $Y$ with respect to time $t$, $u(t)$ is the harmonic excitation signal with frequency $\omega$ and amplitude $d_0$ applied at the top of the cantilever, and finally $f(t)$ is the tip-sample interaction shear force at the tip of the cantilever. Furthermore, the tip sample interaction force at the tip can be split into a viscous and an elastic force [4]:

$$f(t) = -\nu\frac{\partial Y}{\partial t}\bigg|_{\zeta=L} - \kappa Y(L) \quad (6)$$

where $\nu$ is the dissipative or viscous interaction constant and $\kappa$ is the elastic interaction constant.

The model in (1)-(5) provides a first indication of the non-trivial dynamic relationship between the input signals $u(t)$ (the sinusoidal excitation signal), $f(t)$ (the unknown shear force) and the measured output $y(t) = Y(t, \zeta = L)$. The aim in this paper is to estimate the unknown shear force signal $f(t)$ using an unknown input observer technique based only on knowledge of $y(t)$ and $u(t)$. It should be noted that $f(t)$ and $u(t)$ are not collocated. Because of this it is necessary to obtain a (state space) model to relate $u(t)$ and $f(t)$ to $y(t) = Y(t, \zeta = L)$ for estimation of $f(t)$.

## III. Linear differential equation model of the cantilever

In this section, the method of lines will be introduced to approximate the PDE in (1) by a system of linear time-invariant (LTI) ordinary differential equations (ODEs) [37]. This approach also retains some of the versatility of the PDE, as forces and the level of any possible ambient fluid can be modeled with good accuracy by choosing for instance the model parameter $\gamma$ as function of $\zeta$. Most importantly, this approach will provide an accurate control engineering perspective on the influence of the unknown shear force, $f(t)$ (and also the excitation signal $u(t)$) on the output $y(t)$, and the chosen observed states of the system.

The process for obtaining this model is to first conduct a method of lines analysis and then to use an established model reduction approach to obtain a good low order approximation of the dynamic relationship.

### 3.1. Modelling of the cantilever using the method of lines

The main idea is to subdivide the cantilever into $n-1$ equal sections and to consider $n$ nodes distributed along the probe. Denote by $Y_j$ the displacement at node $j$ and let $\delta\zeta$ represent the distance between two consecutive nodes. Using a finite difference formula, the boundary condition (3) for the discretized model becomes

$$\frac{\partial Y}{\partial \zeta}(\zeta = 0) \approx \frac{Y_2 - Y_1}{\delta\zeta} = 0 \tag{7}$$

which implies

$$Y_2 = Y_1. \tag{8}$$

Likewise, the boundary conditions in (4) becomes

$$\frac{\partial^2 Y}{\partial \zeta^2}(\zeta = L) \approx \frac{Y_n - 2Y_{n-1} + Y_{n-2}}{\delta\zeta^2} = 0 \tag{9}$$

or equivalently

$$Y_n - 2Y_{n-1} + Y_{n-2} = 0. \tag{10}$$

Finally (5) can be approximated as

$$\begin{aligned} EI\frac{\partial^3 Y}{\partial \zeta^3}(\zeta = L) &\approx EI_n \frac{Y_n - 3Y_{n-1} + 3Y_{n-2} - Y_{n-3}}{\delta\zeta^3} \\ &= -f(t) \end{aligned} \tag{11}$$

From equations (2), (8), (10) and (11) it is clear that the values of $Y_1, Y_2, Y_n$, and $Y_{n-1}$ are "known", in the sense that they depend on the values of the remaining nodes. Hence, the evolution of the system depends on only $n-4$ nodes. Each of these nodes is described by a second-order ODE. Hence, the dynamics of the cantilever can be represented by a state space system of order of $2(n-4)$. The fourth partial derivative of $Y$ with respect to the spatial variable $\zeta$ can be approximated as

$$\frac{\partial^4 Y_j}{\partial \zeta^4} \approx \frac{Y_{j+2} - 4Y_{j+1} + 6Y_j - 4Y_{j-1} + Y_{j-2}}{\delta\zeta^4} \tag{12}$$

for $j = 3, ..., n-3$. From the boundary conditions for the approximate model, the dynamics of $Y_3, Y_4$ are given by

$$\begin{aligned} \ddot{Y}_3 \;=\; & \frac{1}{\rho A_3}\left(-(\frac{6\alpha EI_3}{\delta\zeta^4} + \gamma_3 w_3)\dot{Y}_3 - \frac{6EI_3}{\delta\zeta^4}Y_3\right. \\ & + \frac{4EI_3}{\delta\zeta^4}(Y_4 + \alpha\dot{Y}_4) - \frac{EI_3}{\delta\zeta^4}(Y_5 + \alpha\dot{Y}_5) \\ & \left. + \frac{3EI_3}{\delta\zeta^4}(u + \alpha\dot{u})\right), \end{aligned} \tag{13}$$

and

$$\begin{aligned} \ddot{Y}_4 \;=\; & \frac{1}{\rho A_4}\left(-(\frac{6\alpha EI_4}{\delta\zeta^4} + \gamma_4 w_4)\dot{Y}_4 - \frac{6EI_4}{\delta\zeta^4}Y_4 + \right. \\ & + \frac{4EI_4}{\delta\zeta^4}(Y_3 + \alpha\dot{Y}_3) + \frac{4EI_4}{\delta\zeta^4}(Y_5 + \alpha\dot{Y}_5) \\ & \left. - \frac{EI_4}{\delta\zeta^4}(Y_6 + \alpha\dot{Y}_6) - \frac{EI_4}{\delta\zeta^4}(u + \alpha\dot{u})\right). \end{aligned} \tag{14}$$

From (8) and (10), it follows

$$Y_{n-1} = 2Y_{n-2} - Y_{n-3} + \frac{\delta\zeta^3}{EI_n}f \tag{15}$$

$$Y_n = 3Y_{n-2} - 2Y_{n-3} + 2\frac{\delta\zeta^3}{EI_n}f. \tag{16}$$

For node $j = n-3$,

$$\begin{aligned} \frac{\partial^4 Y_{n-3}}{\partial \zeta^4} \approx & \frac{1}{\delta\zeta^4}(-2Y_{n-2} + 5Y_{n-3} - 4Y_{n-4} + Y_{n-5} \\ & \left. + \frac{\delta\zeta^3}{EI_n}f\right). \end{aligned} \tag{17}$$

As a result, the dynamics of $Y_{n-3}$ are given by

$$\begin{aligned} \ddot{Y}_{n-3} = & \frac{1}{\rho A_{n-3}}\left(-(\frac{5\alpha EI_{n-3}}{\delta\zeta^4} + \gamma_{n-3}w_{n-3})\dot{Y}_{n-3}\right. \\ & - \frac{5EI_{n-3}}{\delta\zeta^4}Y_{n-3} + \frac{4EI_{n-3}}{\delta\zeta^4}(Y_{n-4} + \alpha\dot{Y}_{n-4}) \\ & - \frac{EI_{n-3}}{\delta\zeta^4}(Y_{n-5} + \alpha\dot{Y}_{n-5}) + \frac{2EI_{n-3}}{\delta\zeta^4}(Y_{n-2} + \alpha\dot{Y}_{n-2}) \\ & \left. - \frac{I_{n-3}}{\delta\zeta I_n}(f + \alpha\dot{f})\right). \end{aligned} \tag{18}$$

Similarly for node $j = n-2$,

$$\frac{\partial^4 Y_{n-2}}{\partial \zeta^4} \approx \frac{1}{\delta\zeta^4}\left(Y_{n-2} - 2Y_{n-3} + Y_{n-4} - 2\frac{\delta\zeta^3}{EI_n}f\right).$$

Thus, the dynamics of $Y_{n-2}$ are described as

$$\begin{aligned} \ddot{Y}_{n-2} = & \frac{1}{\rho A_{n-2}}\left(-(\frac{\alpha EI_{n-2}}{\delta\zeta^4} + \gamma_{n-2}w_{n-2})\dot{Y}_{n-2}\right. \\ & - \frac{EI_{n-2}}{\delta\zeta^4}Y_{n-2} + \frac{2EI_{n-2}}{\delta\zeta^4}(Y_{n-3} + \alpha\dot{Y}_{n-3}) \\ & \left. - \frac{EI_{n-2}}{\delta\zeta^4}(Y_{n-4} + \alpha\dot{Y}_{n-4}) + \frac{2I_{n-2}}{\delta\zeta I_n}(f + \alpha\dot{f})\right). \end{aligned} \tag{19}$$

An ODE for node $j$ $(j = 5, ..., n-4)$ is given by

$$\begin{aligned}\ddot{Y}_j =&\frac{1}{\rho A_j}\Bigg(-(\frac{6\alpha EI_j}{\delta\zeta^4}+\gamma_j wj)\dot{Y}_j \\ &-\frac{6EI_j}{\delta\zeta^4}Y_j-\frac{EI_j}{\delta\zeta^4}(Y_{j-2}+\alpha\dot{Y}_{j-2}+Y_{j+2}+\alpha\dot{Y}_{j+2}) \\ &+\frac{4EI_j}{\delta\zeta^4}(Y_{j-1}+\alpha\dot{Y}_{j-1}+Y_{j+1}+\alpha\dot{Y}_{j+1})\Bigg).\end{aligned} \tag{20}$$

Define state variables as follows:

$$\begin{aligned}x_1 =&Y_3,\\ x_2 =&\dot{Y}_3-\frac{3EI_3}{\rho A_3\delta\zeta^4}\alpha u,\\ x_3 =&Y_4,\\ x_4 =&\dot{Y}_4+\frac{EI_4}{\rho A_4\delta\zeta^4}\alpha u,\\ x_{2n-11} =&Y_{n-3},\\ x_{2n-10} =&\dot{Y}_{n-3}+\frac{I_{n-3}}{\rho A_{n-3}\delta\zeta I_n}\alpha f,\\ x_{2n-9} =&Y_{n-2},\\ x_{2n-8} =&\dot{Y}_{n-2}-\frac{2I_{n-2}}{\rho A_{n-2}\delta\zeta I_n}\alpha f,\end{aligned}$$

and

$$\begin{aligned}x_{2j-5} =&Y_j,\\ x_{2j-4} =&\dot{Y}_j\end{aligned}$$

for $j = 5, ..., n-4$. From these definitions, the LTI system

$$\dot{x}_p = A_p x_p + B_p u + D_p f \tag{21}$$
$$y = C_p x_p \tag{22}$$

where $A_p \in \mathbb{R}^{2(n-4)\times 2(n-4)}$, $B_p \in \mathbb{R}^{2(n-4)\times 1}$ and $D_p \in \mathbb{R}^{2(n-4)\times 1}$ can be constructed. Assuming $\delta\zeta$ is sufficiently small, (21) is a good approximation of the PDE. In (22), the output $y$ is taken as $Y_{n-2}$ and hence the $(2n-9)th$ entry of $C_p \in \mathbb{R}^{1\times 2(n-4)}$ is 1, whilst the remaining entries are zero. Since $Y_n \approx Y_{n-2}$ for large enough $n$, the shear force from (6) can be approximated by

$$\begin{aligned}f(t) \approx& -\nu\frac{\partial Y_{n-2}}{\partial t}-\kappa Y_{n-2}\\ =&-\nu(x_{2n-8}+\frac{2I_{n-2}}{\rho A_{n-2}\delta\zeta I_n}\alpha f)-\kappa x_{2n-9}\end{aligned} \tag{23}$$

or

$$f(t) \approx -\left(\frac{1}{1+\nu\alpha\frac{2I_{n-2}}{\rho A_{n-2}\delta\zeta I_n}}\right)(\nu x_{2n-8}+\kappa x_{2n-9})$$

Note that the $\kappa$ and $\nu$ are unknown and vary with tip/specimen distance.

### 3.2. Reduced order model

When $n$ is large, the model in (21) is a good approximation of the real PDE - but at the cost of significant computation. Since a high order system is not convenient for computation, particularly for on-line implementation (which is the ultimate goal of the project), a model reduction technique will be employed to create a more manageable lower order model. There is of course a significant amount of literature on this topic, and a wide range of model reduction methods could be employed [44]. In this paper, the standard balanced truncation method by Moore [33], which is available in Matlab, has been used. Hence, for observer design, a model of the form

$$\dot{x}(t) = Ax(t)+Bu(t)+Df(t) \tag{24}$$
$$y(t) = Cx(t) \tag{25}$$

where $x \in \mathbb{R}^{n_r}$ will be used. The order of the system in (24), represented by $n_r$, is by construction significantly lower than $n$.

## IV. Sliding mode observer

A sliding mode observer will then be presented to reconstruct the tip-sample interaction shear force. The above model (24) will be used for the design of the sliding mode observer to estimate the shear force $f(t)$ from knowledge of only $y(t)$ and $u(t)$. In the literature, numerous methods for designing sliding mode observers have appeared [14,15,39]. In this paper, the design will be based on the sliding mode observer proposed in [14] for square systems. This particular sliding mode observer has the structure

$$\dot{\hat{x}}(t) = A\hat{x}(t)+Bu(t)-Ge_y(t)+Dv \tag{26}$$
$$\hat{y}(t) = C\hat{x}(t) \tag{27}$$

where the output estimation error

$$e_y(t) = \hat{y}(t)-y(t). \tag{28}$$

The objective of the observer is to drive $e_y$ to zero in finite time [11, 40]. In (26) the gain $G$ must be chosen

so that there exists a symmetric positive definite matrix $P$ such that

$$P(A-GC)+(A-GC)^T P<0 \tag{29}$$

and

$$PD=(FC)^T \tag{30}$$

for some $F\in\mathbb{R}$. This is essentially the observer initially proposed by Walcott & Zak [41]. The nonlinear injection signal in (26) is given by

$$v=\begin{cases} -\sigma\frac{Fe_y}{\|Fe_y\|} & \text{if } e_y\neq 0,\\ 0 & \text{otherwise}\end{cases} \tag{31}$$

and the scalar gain $\sigma$ must satisfy

$$\|f(t)\|\leq\sigma. \tag{32}$$

In order for an observer of the form (26)-(31) to exist for the particular problem under consideration, the following conditions must be satisfied [11, 13]:

- rank$(CD)=1$ or in this case $CD\neq 0$
- invariant zeros of $(A,D,C)$ must lie in $\mathbb{C}_-$

Here because the system is square, an analytic solution to the design problem can be employed. Specifically, in this paper, the approach proposed in [14] will be employed to compute $G$. Despite the model reduction employed to create $(A,D,C)$, the resulting state space is of order 9, and more importantly badly numerically conditioned. The approach in [14] does not employ any numerical transformations of the state-space (compared to [11] for example) and this is advantageous here. The only transformation required is an orthogonal one to obtain a specific "regular form" for the pair $(A,D)$ [11]. Based on QR decomposition of the matrix $D$, there exists a linear orthogonal change of coordinates $x\mapsto\chi=\text{col}(\chi_1,\chi_2)=Tx$ such that in the new coordinate system

$$\dot\chi_1(t) = A_1\chi_1(t)+A_2\chi_2(t)+B_1u(t) \tag{33}$$
$$\dot\chi_2(t) = A_3\chi_1(t)+A_4\chi_2(t)+B_2u(t)+D_2f(t) \tag{34}$$
$$y(t) = C_1\chi_1(t)+C_2\chi_2(t) \tag{35}$$

where $\chi_1\in\mathbb{R}^{n_r-1}$, $\chi_2\in\mathbb{R}$ and the matrix sub-blocks $A_1,\ldots,A_4$ have no structure. Note that in (34), the scalar satisfies $D_2\neq 0$. As argued in [14], in the regular form coordinates, a suitable choice for the observer gain is

$$G=\begin{bmatrix} A_2C_2^{-1} \\ A_4C_2^{-1}-C_2^{-1}A_4^s\end{bmatrix} \tag{36}$$

where $A_4^s$ is a negative design scalar. For details see [14]. Note that $C_2\neq 0$ since $CD=C_2D_2$ and $CD\neq 0$ by assumption. The scalar $F$ from (31) can be parameterised in the form

$$F=P_2C_2D_2 \tag{37}$$

for some positive scalar $P_2$. In the new coordinates, the state estimation error $\text{col}(e_1,e_2)=\chi-\hat\chi$, for $\hat\chi=T\hat x$, satisfies

$$\dot e_1(t)=(A_1-A_2C_2^{-1}C_1)e_1(t) \tag{38}$$
$$\dot e_2(t)=\tilde A_3e_1(t)+C_2^{-1}A_4^sC_2e_2(t)+D_2(f(t)-v) \tag{39}$$

where $\tilde A_3=A_3-A_4C_2^{-1}C_1-C_2A_4^sC_1$. During sliding, $e_y=0$ and $\dot e_y=0$ [11, 40] and thus $e_2=\dot e_2=0$. From (39) it follows that

$$v_{eq}=f+D_2^{-1}\tilde A_3e_1(t) \tag{40}$$

where $v_{eq}$ is the so-called "equivalent injection" necessary to maintain a sliding motion [11, 40]. Since the eigenvalues of $(A_1-A_2C_2^{-1}C_1)$ are the invariant zeros of $(A,D,C)$, the subsystem (38) is stable by assumption and $e_1(t)\to 0$ as $t\to\infty$. Therefore from (40) the injection signal

$$v_{eq}\to f(t) \tag{41}$$

In practice the equivalent injection $v_{eq}$ (and hence the shear force $f(t)$), can be extracted from (31) by using a low-pass filter [40]. In the paper, a first order low pass filter of the form

$$\dot{\tilde v}=-k\tilde v+kv,\quad k>0,\ \tilde f(0)=0 \tag{42}$$

is used to obtain the force estimate (i.e the equivalent injection). For a large value of $k$, it follows that $\tilde v\approx v_{eq}\to f(t)$. Consequently using the sliding mode observer, changes in the shear force $f(t)$ can be estimated in real time as the tip descends towards the sample through the ordered water layers. However, a more succinct indication of these changes can be observed from changes in the shear force model parameters $\kappa$ and $\nu$ from (6). In addition to estimating $f(t)$ in real time, this information will be used to estimate $\kappa(t)$ and $\nu(t)$ from the model given in (6) via least squares [36]. In (6), the left hand side is available from the equivalent injection signal which is extracted using the low-pass filter in (42). Consequently to obviate the effect of any phase lag associated with the filter, all time dependent terms on the right hand side of (6) will also be subject to the same filter, specifically:

$$\dot{\tilde Y}=-k\tilde Y+kY(L),\ \tilde Y(0)=0. \tag{43}$$

Then it follows from (6) that

$$\tilde{f}(t) = -\nu\frac{\partial\tilde{Y}}{\partial t} - \kappa\tilde{Y} \tag{44}$$

Furthermore, (43) can be used to obtain $\frac{\partial\tilde{Y}}{\partial t}$, i.e. as $-k\tilde{Y} + kY$. Consequently no measured knowledge of $\frac{\partial\tilde{Y}}{\partial t}$ is required (see for example [31, 34, 36]). Adaptive estimation procedures can then be used to estimate $\kappa$ and $\nu$ [31, 34].

**Remark IV.1** *The combination of sliding mode observers and least squares methods has previously appeared in the literature: see for example [5]. However, here the formulation is quite bespoke for the TDFM problem. The use of the low-pass filters and the ideas of [31, 34, 36] allow the estimation of the shear force model parameters based only on the estimates of $f(t)$ and measurements of $Y(L)$.*

## V. Practical Results

In the Bristol TDFM, the particular cantilever used is made of Silicon Nitride (Si3N4) by NuNano (http://www.nunano.com/). The parameters are given by: Young's modulus E=210 GPa, $\rho$=3100 kg/m$^3$, length L=28 $\mu$m, width w=2 $\mu$m, thickness $t_c = 200$ nm. The cantilever is brought into the proximity of a quartz cover glass slide under normal room conditions, without using any additional fluid as medium (i.e. $\gamma = 0$). Thus, a small water layer of less than 10 nm is to be expected on the glass slide surface due to environmental humidity. This paper presents four data sets $X_1$, $X_2$, $X_3$, and $X_4$ comprising input and output signals collected from the experimental setup associated with tip-to-surface distances corresponding to 2 nm, 5 nm, 7 nm, and 8 nm respectively. The top of the cantilever was excited close to its first resonance frequency of 352.750 kHz. The amplitude of the excitation signal is 1.8 nm.

The input and output signals are shown in Figures 6 - 7. Since the signals contain noise, band pass filters have been employed with the bandwidth covering the excitation frequency. The scaling factors required to recover the measured signals in SI units were calculated based on the frequency responses of the input and output signals when the data was collected at a distance of 9 nm (considered as far) from the glass. At low frequencies, in which the phase values are close to zero, the magnitude of the frequency response corresponds to 1. At the excitation signal, the magnitude of the frequency response is equal to the magnitude of the transfer function of the discretization model (21), which helps to calculate the scaling factor.

Here the number of nodes used in the method of lines was chosen as $n = 100$. This is a result of an empirical analysis of the model in relation to the first resonance frequency of 352.750 kHz and the general shape of the frequency response $G_{pu}(s) = C_p(sI - A_p)B_p$ for different value of $n$. Figure 3 shows Bode diagrams of the original PDE and the high order LTI models obtained from the method of lines. For smaller values of $n$, the method of lines models have a high value for the first resonance frequency. It appears to be 'stiff' for a lower value of $n$. As $n$ increases, the value of the actual resonance frequency of 352.750 kHz is approached. Figure 4 provides Bode plots of

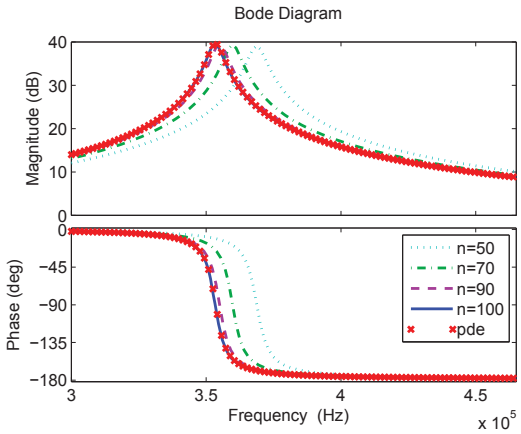


Fig. 3. Discretized Bode diagrams for $G_{pu}(s)$ for different values of $n$

both the transfer functions $G_{pu}(s) = C_p(sI - A_p)B_p$ and $G_{pf}(s) = C_p(sI - A_p)D_p$ across a large frequency range. Although both systems share the same state space, the input-output behaviour of both systems is non-trivially different. This is not only true for the low frequency range but also for the frequency range around the first (and second) resonance frequency and the relevant gain (and phase) behaviour. This is clearly related to very different zero-dynamics behaviour and the fact that $f(t)$ and $u(t)$ are not collocated. The suggested modelling approach ensures that this is reflected in the overall state space model (24)-(25) (see also (21)).

The Matlab function "modred" was employed to generate a reduced-order model of order $n_r = 9$, (which is based on the balanced truncation method by Moore [33]). The Matlab function "balreal" was also used to improve the conditioning of the state-space representation for implementation. The 9 largest Hankel

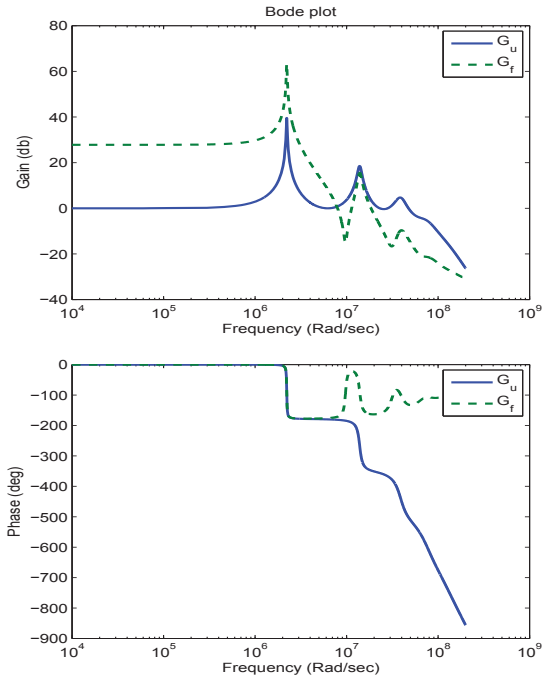


Fig. 4. Magnitude and Phase Plot of $G_{pu}(s) = C_p(sI - A_p)B_p$ and $G_{pf}(s) = C_p(sI - A_p)D_p$

singular values preserved in the reduced model are: 734.6345, 722.6798, 5.3423, 4.8253, 0.9912, 0.8024, 0.2473, 0.2088, 0.0414. The model mismatch between the discretized model and the reduced-order one is

$$\|H(s) - H_r(s)\|_\infty = 0.0697 \tag{45}$$

where $H(s)$ is the transfer function of the discretized model in (21) and $H_r(s)$ is the transfer function of the reduced-order model from (24). Furthermore, $\|H(s)\|_\infty = 1457.4743$ and $\|H_r(s)\|_\infty = 1457.4758$ and hence the error in (45) is relatively small, and the reduced-order model is considered reliable. Figure 5 shows Bode diagrams of the original PDE, the high order LTI model obtained from the method of lines, and the 9th order model used for the design of the observer, over a frequency range about the 1st flexural frequency. It is clear that there is a good fit between the reduced order model used for the observer design and the PDE (in the frequency range of interest).

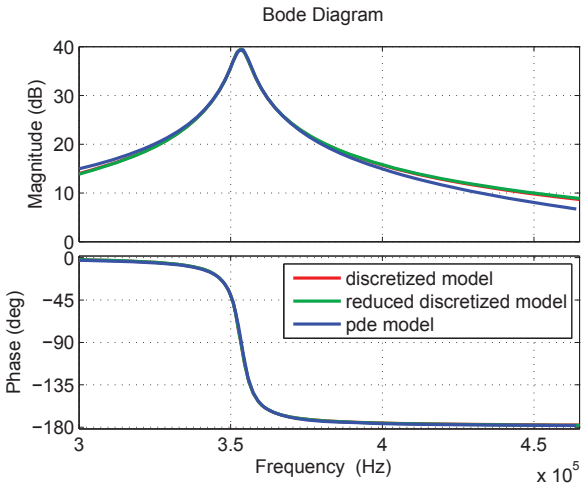


Fig. 5. Bode diagrams for $G_u = C(sI - A)B$ of the order reduced model, discretized & PDE derived frequency response

The parameters for the observer (26) were chosen as: $\sigma = 2000$, $A_4^s = -10^9$, and

$$G = \begin{bmatrix} 849698.1752 \\ 830497.8541 \\ -280876.6790 \\ 22948.7125 \\ -128982.3488 \\ 1589.1755 \\ 8361.6753 \\ -4507.1457 \\ 8661.2590 \end{bmatrix}.$$

A typical example of the sinusoidal excitation signal applied to the top of the cantilever is shown in Figure 6. The position signals of the tip of the cantilever, for each of the four data sets, are shown in Figure 7. Figure 8 shows the output estimation error $e_y(t)$ for data set $X_1$ (which is typical of the ones obtained for $X_2$, $X_3$ and $X_4$). Since the signal $e_y$ is of order $10^{-5}$ compared to the output signals themselves, this demonstrates that the sliding mode observer performs well and accurately tracks the measured signal in each case. The shear force estimates are shown in Figure 9 which exhibit noisy sinusoidal-like signals with the same underlying frequency as the excitation signal $u(t)$. It is clear that the shear force corresponding to the data set $X_1$ exhibits the largest interaction with the sample, i.e. it has the largest amplitude among the shear forces. This agrees with the fact that the shear force is larger when the tip is put closer to the sample on the glass surface.

In the tests, it can be noticed that the elastic component $\kappa\tilde{Y}$ in the overall shear force is negligible

(44) so that only the viscous coefficient $\nu$ was estimated as depicted in Figure 10. Estimates are obtained with an initial settling time of less than 50 $\mu$s, which is due to the combined dynamics of the observer, together with the various low and band-pass filters. From thereon, highly dynamic real-time results (settling faster than 50 $\mu$s) are obtained. The viscous coefficient clearly increases in value as the distance to the glass surface decreases, i.e. considering case $X_4$ as the farthest from the glass surface.

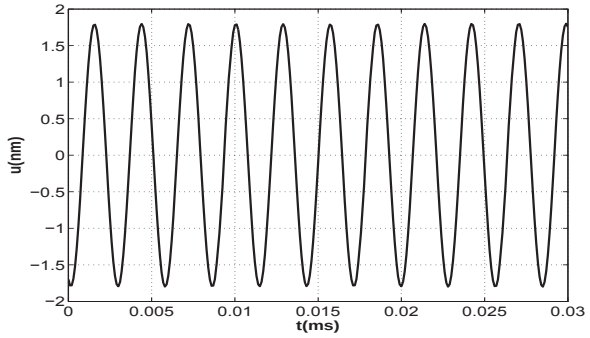


Fig. 6. A typical input signal applied at the top of the cantilever (technically for data $X_1$)

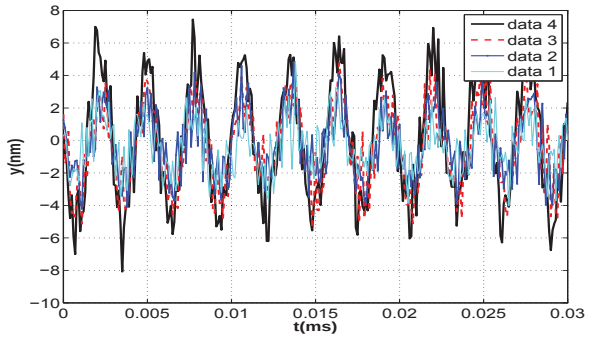


Fig. 7. Output signals

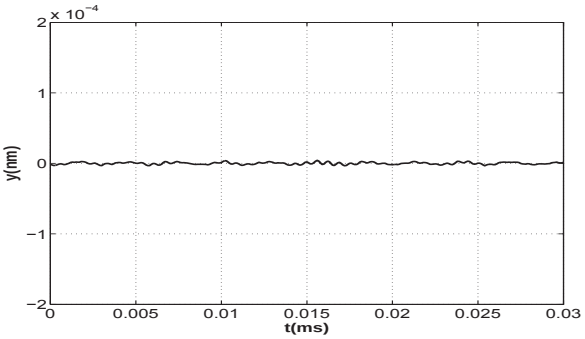


Fig. 8. A typical output estimation error $e_y$ (technically for data $X_1$)

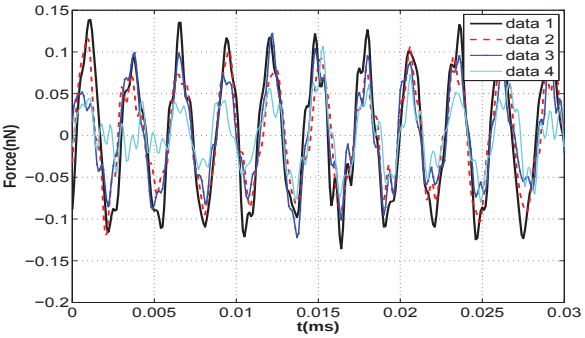


Fig. 9. Estimate of shear force

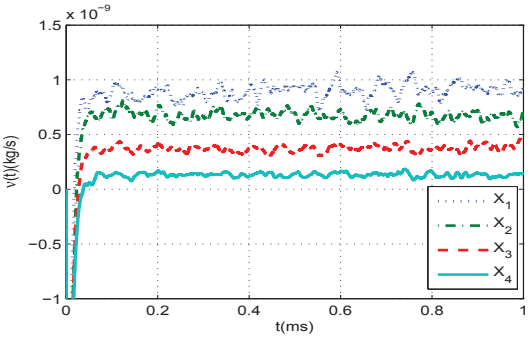


Fig. 10. Estimate of the viscous coefficient $\nu$ for the 4 different cases

## VI. Conclusion

It has been shown that it is possible to obtain real-time estimates of the shear forces affecting the vertically oriented cantilever in Bristol's TDFM. This information has been complemented by a parametric representation of the shear force, in terms of elastic and dissipative constants, which gives a scaled measure of the cantilever-specimen distance. These estimates of the shear force have been obtained using a sliding mode observer and by considering the problem as a classical unknown input formulation. It has been shown that it is sufficient to use a reduced order model, derived from an approximate ODE model of the cantilever dynamics, as the basis for the observer design. Experimental results have been presented based on tests carried out on the TDFM rig at the Centre for NSQI at Bristol. The results confirm an increasing shear force and viscous coefficient with closer proximity of the cantilever tip to the bottom glass slide.

## REFERENCES


1. T. Ando. Control techniques in high-speed atomic force microscopy. In *American Control Conference, 2008*, pages 3194 –3200, june 2008.
2. M. Antognozzi, D.R. Binger, A.D.L. Humphris, P.J. James, and M.J. Miles. Modeling of cylindrically tapered cantilevers for transverse dynamic force microscopy (TDFM). *Ultramicroscopy*, 86(1-2):223 – 232, 2001.
3. M. Antognozzi, A. Ulcinas, L. Picco, S.H. Simpson, P.J. Heard, M.D. Szczelkun, B.Brenner, and M.J. Miles. A new detection system for extremely small vertically mounted cantilevers. *Nanotechnology*, 19(38):384002, 2008.
4. M. Antognozzi. *Investigation of the shear force contrast mechanism in transverse dynamic force microscopy*. PhD thesis, Univeristy of Bristol, 2000.
5. S. Baev, I. Shkolnikov, Y. Shtessel, and A. Poznyak. Sliding mode parameter identification of systems with measurement noise. *International Journal of Systems Science*, 38:871–878, 2007.
6. G. Besancon, A. Voda, and M. Alma. On observer-based estimation enhancement by parametric amplification in a weak force measurement device. In *Decision and Control, 2008. CDC 2008. 47th IEEE Conference on*, pages 5200 – 5205, 2008.
7. N. A. Burnham and R. J. Colton. Measuring the nanomechanical properties and surface forces of materials using an atomic force microscope. *Journal of Vacuum Science Technology*, 1989.
8. M. Corless and J. Tu. State and input estimation for a class of uncertain systems. *Automatica*, 34:757–764, 1998.
9. M. Darouach. On the novel approach to the design of unknown input observers. *IEEE Transactions on Automatic Control*, 39:698–699, 1994.
10. T. De, P. Agarwal, D.R. Sahoo, and M.V. Salapaka. Real-time detection of probe loss in atomic force microscopy. *Applied Physics Letters*, 89(13):133119–1–133119–3, 2006.
11. C. Edwards and S.K. Spurgeon. *Sliding Mode Control: Theory and Applications*. Taylor & Francis, 1998.
12. C. Edwards and C.P. Tan. A comparison of sliding mode and unknown input observers for fault reconstruction. *European Journal of Control*, 14, 2006.
13. C. Edwards, X.G. Yan, and S.K. Spurgeon. On the solvability of the constrained lyapunov problem. *IEEE Transactions Automatic Control*, 52:1982–1987, 2007.
14. C. Edwards and S.K. Spurgeon. Sliding mode output tracking with application to a multivariable high temperature furnace problem. *International Journal of Robust and Nonlinear Control*, 7(4):337–351, 1997.
15. C. Edwards, S.K. Spurgeon, and R.J. Patton. Sliding mode observers for fault detection and isolation. *Automatica*, 36(4):541 – 553, 2000.
16. S. Eslami and N. Jalili. Adaptive trajectory control of microcantilever's tip utilised in atomic force microscopy-based manipulation. *International Journal of Control*, 84(12):1945–1955, 2011.
17. S. Eslami and N. Jalili. Automated boundary interaction force control of micromanipulators with in situ applications to microsurgery. *Journal of Micromechanics and Microengineering*, 22(12):125013, 2012.
18. S. Faegh and N. Jalili. Comprehensive distributed-parameters modeling and experimental validation of microcantilever-based biosensors with an application to ultrasmall biological species detection. *Journal of Micromechanics and Microengineering*, 23(2):025007, 2013.
19. Y.C. Fang, M. Feemster, D. Dawson, and N.M. Jalili. Nonlinear control techniques for an atomic force microscope system. *Journal of Control Theory and Applications*, 3(1):85–92, 2005.
20. Y.C. Fang, M.G Feemster, D.M. Dawson, and N. Jalili. Nonlinear control techniques for the atomic force microscope system. In *ASME 2002 International Mechanical Engineering Congress and Exposition*, pages 373–380. American Society of Mechanical Engineers, 2002.
21. G.E. Fantner, G. Schitter, J.H. Kindt, T. Ivanov, K. Ivanova, R. Patel, N. Holten-Andersen, J. Adams, P.J. Thurner, I.W. Rangelow, and P.K. Hansma. Components for high speed atomic force microscopy. *Ultramicroscopy*, 106(8-9):881 – 887, 2006.
22. L. Fridman, A. Levant, and J. Davila. High-order sliding-mode observation and identification for linear systems with unknown inputs. In *Proceedings of the IEEE Conference on Decision and Control, San Diego, CA*, pages 5567–5572, 2006.
23. T. Fukuma, M. Kimura, K. Kobayashi, K. Matsushige, and H. Yamada. Development of low noise cantilever deflection sensor for multi-environment frequency-modulation atomic force microscopy. *Review of Scientific Instruments*, 76:053704, 2005.

24. B.Z. Guo and Z.L. Zhao. On the convergence of an extended state observer for nonlinear systems with uncertainty. *Systems & Control Letters*, 60(6):420–430, 2011.
25. P.K. Hansma, G. Schitter, G.E. Fantner, and C. Prater. High-speed atomic force microscopy. *Science*, 314(5799):601–602, 2006.
26. R L Harniman, J A Vicary, J K H Hörber, L M Picco, M J Miles, and M Antognozzi. Methods for imaging dna in liquid with lateral molecular-force microscopy. *Nanotechnology*, 23(8):085703, 2012.
27. R. Howland and L. Benatar. *Practical Guide to Scanning Probe Microscopy*. Park Scientific Instruments: Sunnyvale, CA, USA, 1993.
28. H.K. Khalil. High-gain observers in nonlinear feedback control. In *International Conference on Control, Automation and Systems, 2008. ICCAS 2008.*, pages xlvii–lvii, 2008.
29. N. Kodera, H. Yamashita, and T. Ando. Active damping of the scanner for high-speed atomic force microscopy. *Review of Scientific Instruments*, 106:053708, 2005.
30. S. Kuiper and G. Schitter. Improving the imaging speed of afm with modern control techniques. In Evangelos Eleftheriou and S. Moheimani, editors, *Control Technologies for Emerging Micro and Nanoscale Systems*, volume 413 of *Lecture Notes in Control and Information Sciences*, pages 83–100. Springer Berlin / Heidelberg, 2011.
31. M.N. Mahyuddin, J. Na, G. Herrmann, X. Ren, and P. Barber. Adaptive observer-based parameter estimation with application to road gradient and vehicle mass estimation. *IEEE Transactions on Industrial Electronics*, 61(6):2851–2863, 2014.
32. A. Marcos, S. Ganguli, and G.J. Balas. An application of h-infinity fault detection and isolation to a transport aircraft. *Control Engineering Practice*, 13(1):105–119, 2005.
33. B. Moore. Principal component analysis in linear systems: Controllability, observability, and model reduction. *IEEE Transactions on Automatic Control*, 26(1):17 – 32, 1981.
34. J. Na, M. Mahyuddin, G. Herrmann, and X. Ren. Robust adaptive finite-time parameter estimation for linearly parameterized nonlinear systems. In *32nd Chinese Control Conference (CCC)*, pages 1735–1741, 2013.
35. K.A. Ramirez-Aguilar and K.L. Rowlen. Tip characterization from afm images of nanometric spherical particles. *Langmuir*, 14(9):2562–2566, 1998.
36. S. Sastry and M. Bodson. *Adaptive Control: Stability, Convergence, and Robustness*. Prentice-Hall, 1994.
37. W. E. Schiesser and G. W. Griffiths. *A Compendium of Partial Differential Equation Models: Method of Lines Analysis with Matlab*. Cambridge University Press, Cambridge, 2009.
38. G. Schitter, P.J. Thurner, and P.K. Hansma. Design and input-shaping control of a novel scanner for high-speed atomic force microscopy. *Mechatronics*, 18(56):282 – 288, 2008.
39. C.P. Tan and C. Edwards. Robust fault reconstruction in uncertain linear systems using multiple sliding mode observers in cascade. *IEEE Transactions on Automatic Control*, 55(4):855 – 867, 2010.
40. V.I. Utkin. *Sliding Modes in Control Optimization*. Springer-Verlag, Berlin, 1992.
41. B.L. Walcott and S.H. Żak. State observation of nonlinear uncertain dynamical systems. *IEEE Transaction on Automatic Control*, 32:166–170, 1987.
42. B.L. Walcott, M.J. Corless, and S.H. Żak. Comparative study of nonlinear state observation techniques. *International Journal of Control*, 45:2109–2132, 1987.
43. X. Xu, J. Melcher, and A. Raman. Accurate force spectroscopy in tapping mode atomic force microscopy in liquids. *Phys. Rev. B*, 81:035407–1–035407–7, 2010.
44. K. Zhou, J.C. Doyle, and K. Glover. *Robust and Optimal Control*. Prentice Hall, New Jersey, 1996.